International Conference on Space Optics—ICSO 2006

Noordwijk, Netherlands

27–30 June 2006

Edited by Errico Armandillo, Josiane Costeraste, and Nikos Karafolas

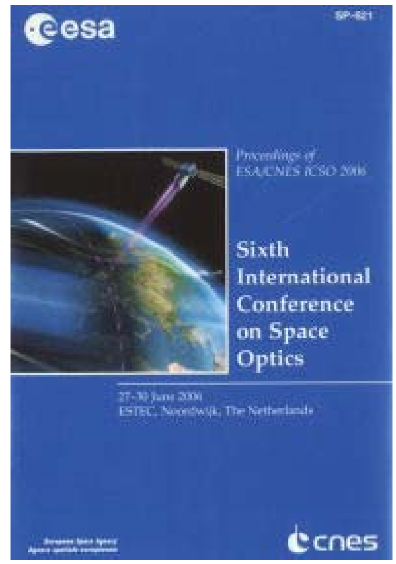

PEGASE: a free flying interferometer for the spectroscopy of giant exo-planets

J.-M. Le Duigou, M. Ollivier, A. Léger, F. Cassaing, et al.

International Conference on Space Optics — ICSO 2006, edited by Errico Armandillo, Josiane Costeraste,
Nikos Karafolas, Proc. of SPIE Vol. 10567, 1056702 · © 2006 ESA and CNES
CCC code: 0277-786X/17/$18 · doi: 10.1117/12.2308110

PEGASE: A FREE FLYING INTERFEROMETER FOR THE SPECTROSCOPY OF GIANT EXO-PLANETS

J.M. Le Duigou[(1)*], M. Ollivier[(2)], A. Léger[(2)], F. Cassaing[(3)], B. Sorrente[(3)], B. Fleury[(3)], G. Rousset[(3,7)], O. Absil[(4)], D. Mourard[(5)], Y. Rabbia[(5)], L. Escarrat[(5)], F. Malbet[(6)], D. Rouan[(7)], R. Clédassou[(1)], M. Delpech[(1)], P. Duchon[(1)], B. Meyssignac[(1)], P.-Y. Guidotti[(1)], N. Gorius[(1)]

* *Jean-Michel.LeDuigou@cnes.fr*

[(1)] *Centre National d'Etudes Spatiale (CNES),* [(2)] *Institut d'Astrophysique Spatiale (IAS),*
[(3)] *Office National d'Etudes et de Recherches Aéronautiques (ONERA),* [(4)] *Université de Liège,*
[(5)] *Observatoire de la Côte d'Azur (OCA),* [(6)] *Laboratoire d'Astrophysique de l'Observatoire de Grenoble (LAOG),*
[(7)] *Observatoire de Paris*

ABSTRACT

This paper presents a summary of the phase-0 performed in 2005 for the Pegase mission. The main scientific goal is the spectroscopy of hot Jupiters (Pegasides) and brown dwarfs from 2.5 to 5 µm. The mission can extend to the exploration of the inner part of protoplanetary disks, the study of dust clouds around AGN,... The instrument is basically a two-aperture (D=40 cm) interferometer composed of two siderostats and one beam-combiner. The formation is linear and orbits around L2, pointing in the anti-solar direction within a +/-30° cone. The baseline is adjustable from 50 to 500 m in both nulling and visibility measurement modes. The angular resolution ranges from 1 to 20 mas and the spectral resolution is 60. In the nulling mode, a 2.5 nm rms stability of the optical path difference (OPD) and a pointing stability of 30 mas rms impose a two level control architecture. It combines control loops implemented at satellite level and control loops operating inside the payload using fine mechanisms. According to our preliminary study, this mission is feasible within an 8 to 9 years development plan using existing or slightly improved space components, but its cost requires international cooperation. Pegase could be a valuable Darwin/TPF-I pathfinder, with a less demanding, but still ambitious, technological challenge and a high associated scientific return.

1. INTRODUCTION

In 2004, CNES issued a call for scientific proposals for space based formation flying missions. A consortium led by IAS and including other scientific laboratories and Alcatel Space, proposed the Pegase mission [1]. It was selected to proceed to a phase 0 process in 2005. This paper summarizes the work performed in this framework by a joint team of CNES and ONERA engineers and scientists from various laboratories. For the interested readers, an associated paper of the same conference [2] gives a more detailed description of the optical payload and the fine control loops.

2. SCIENTIFIC OBJECTIVES

2.1 - Hot Jupiters

During the past decade, the indirect ground based observations proved the existence of more than 150 giant exo-planets. A special class is composed by hot Jupiters which orbit very close around their parent star (from 0.05 to 0.1 AU). Their mass varies from 0.11 to 10 mass of Jupiter (MJ) and their temperature reaches 700 to 1500 K. Their formation process remains poorly understood and there is now room for a new science aiming at a better understanding of such objects. The Corot and Kepler missions, thanks to the transit detection method combined with available ground information, will provide us with precise estimates of the mass and the radius of such objects. The Pegase mission is interested by the next step which is the spectral characterization of hot Jupiters (also called Pegasides, which give the name of the mission). The current models need to be constrained by measurements to better characterize the physics of their atmosphere: the chemical composition, the amount of thermalization, the existence of local winds, the importance of clouds,…The main molecular signatures of interest (CH_4, H_2O, CO, see Fig. 1) lie in the 1.5-5 µm range. The required spectral resolution is moderate (R=60) and the minimum SNR is 10.

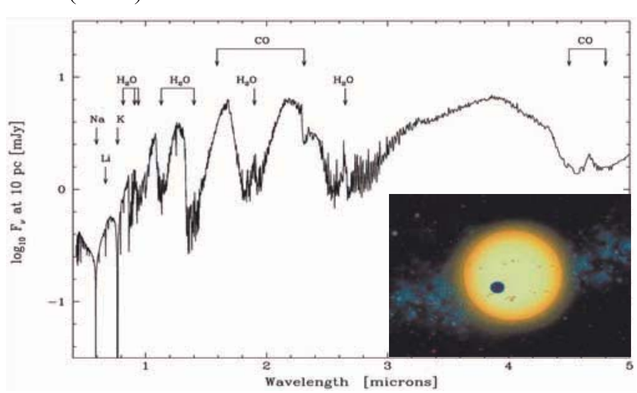

Fig. 1: atmospheric model of hot Jupiters [3], [4]

Proc. '6th Internat. Conf. on Space Optics', ESTEC, Noordwijk, The Netherlands, 27-30 June 2006 (ESA SP-621, June 2006)

The main instrumental challenge is to achieve a very high angular resolution (0.5 to 5 mas) together with a high extinction power of the parent star light. The contrast (star/planet flux ratio) ranges from 10^3 to a few 10^4 in the considered wavelength range. As the desired angular resolution at 2.5-5 µm implies aperture dimensions of several hundred meters and the terrestrial atmospheric absorption limits the ground based observations to some narrow bands, a space based free flying interferometer is proposed. The desired extinction can be implemented using the Bracewell set up [5], i.e. a Michelson interferometer with a π achromatic phase shift in one arm and a rotation of the baseline around the line of sight. Fig. 2 shows how this concept projects a dark fringe on the central parent star while the baseline is adjusted so that a bright fringe coincides with the supposed weak companion elongation. As shown by many authors [6], [7], this concept can not be directly applied to the telluric exo-planets spectral characterization in the mid IR because the nulling ratio of a two apertures system is insufficient to face the 10^6 contrast at 10 µm and a centro-symetric sub-aperture pattern can not extract the exo-planet signal from the exo-zodiacal light. These restrictions no more apply in the case of Pegase because the planet flux is much stronger and the exo-zodiacal light weaker in the selected wavelength range. From the initial list, 16 hot Jupiters were identified as good candidates for the mission. This number may increase in the next years, but will reach a maximum when all nearby stars will have been scanned by indirect methods.

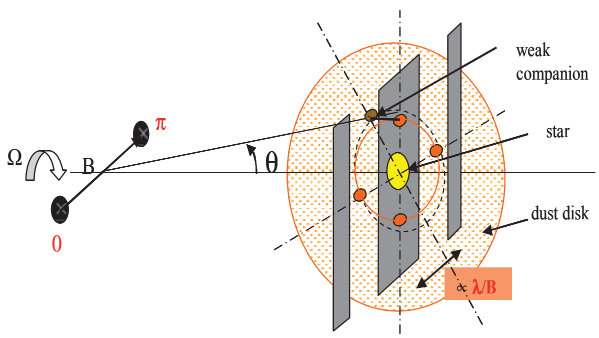

Fig. 2: basic principle of a Bracewell interferometer

2.2 – Brown dwarfs

Reducing the size of the baseline to adapt to greater elongations (10 to 100 mas), the same instrument can also characterize the atmosphere of brown dwarfs using nulling interferometry. This is the second main objective of Pegase which consists mainly in exploring the brown dwarfs desert and constraining the current models of these objects: the relationship between the effective temperature and the radius as a function of mass, the importance of the atmosphere, and especially of CH_4 and clouds. The brown dwarfs have the same kind of characteristic spectral signatures as compared to the hot Jupiters, but their mass lies in the 10 to 80 MJ range. The contrast with the parent star depends on the mass of the brown dwarf and of the age of the system. For masses between 15 and 80 MJ and systems younger than 1 billion years, the contrast ranges from 10^3 to 10^4. Furthermore, the measurements have to be combined with a precise mass estimate to test the coherence of the atmosphere and internal structure models. These requirements limit currently the number of possible targets to a few ones. But future on ground observations will probably extend the list.

2.3 – Other objectives

If the nulling mode is complemented by a more classical but very precise interferometry mode measuring the visibility of the fringes (V^2 mode), one can adapt the Pegase instrument to various other valuable scientific objectives such as the study of circumstellar disks, the study of dust distribution around AGN, the measure of the distance of the Magellan cepheids, the study of massive hydrogen clouds in front of quasars,… To study the V^2 mode in the phase 0, we selected one of the most interesting features: the possible detection of gaps in protoplanetary disks around T-Tauri and Herbig He-Be stars located in star formation regions like the Taurus one (150 pc). Most of the recent studies tend to indicate that the planets formation process begins well before the parent star reaches the main sequence, with probable migrations from the external to the internal regions. During this process each planet should create a characteristic signature, such as a gap, in the dust cloud that slightly modifies the IR emission. Hence, the detailed study of circumstellar disks around young objects is a good test for the presence of planets if one can precisely detect such gaps. Preliminary simulations show that a 0.05 AU gap induces variations of the visibility of a few % (see Fig. 3).

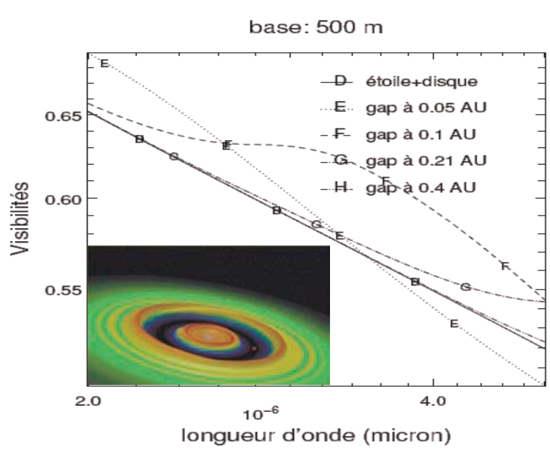

Fig. 3: variations of the visibility induced by a 0.05 AU gap around a T-Tauri tar (CTSS model) B=500 m

3. - SNR CALCULATIONS

Simplified SNR calculations were performed in the scientific laboratories and at CNES with very consistent results. As an example, we detail here below the case of the observation of the hot Jupiters in the nulling mode. Some numerical results are provided in a reference case which is the observation at 3 µm of Ups And b with the parameters listed below Fig. 4.

We suppose that the size and orientation of the baseline are adjusted to the previously known planet elongation so that we have a maximum transmission at 2.5 µm on the planet. Another major assumption is the use of single mode fibers to clean the wavefronts and relax the constraints on optical surfaces [8]. This process converts differential wavefront errors into intensity mismatch [9] which have less impact on the nulling performance than phase errors. After spatial filtering, the residual star light, the planet light and the environmental noises are focused on one pixel for each spectral channel. The average values of noises are removed by a calibration process which includes measurements with at least two angular positions around the line of sight.

The emission of the planet in one spectral channel of width $\Delta\lambda$ is modelled by the following equation:

$$I_p \approx K\left[\frac{A_p R_p^2}{4a_p^2}\left(\frac{R_*}{d}\right)^2 B_\lambda(T_*) + \left(\frac{R_p}{d}\right)^2 S_p(\lambda)\, B_\lambda(T_p)\right] \quad (1)$$

$$\text{with} \quad K = \pi\eta_o(\lambda)\eta_q(\lambda)\eta_p(\lambda,B)\, A\, \Delta\lambda$$

$\eta_p(\lambda,B)$ is the interferometric transmission at the elongation of the planet: $\eta_p(\lambda,B)=2\sin^2(X)$ with $X=\pi B\Delta\theta_*/\lambda$. T_p and T_* are respectively the planet and star effective temperature, R_p and R_* the associated radius, S_p the absorption spectrum, A_p the albedo coefficient, a_p the planet elongation, $\eta_o(\lambda)$ the optical transmission, $\eta_q(\lambda)$ the quantum efficiency of the detector, A the collecting area, B the baseline. $B_\lambda(T)$ is the Planck function. In the reference case $\langle I_p\rangle = 23$ e^-/s.

The main noise sources are the stellar leakage, the detector noise, the thermal noise of the optics and the shot noise. The exo-zodiacal light in 2.5-5 µm is negligible. The local zodiacal light was taken into account according [10] but has a negligible effect in our case because it is supposed constant and is less than 1 e^-/s. Our preliminary analysis does not consider any stray light from the sun, the moon or the earth.

As the nulling is not perfect, some star light reaches the detector, resulting in a stellar leakage:

$$I_* = \pi\eta_o(\lambda)\eta_q(\lambda)\eta_*(\lambda,B)\, A\left(\frac{R_*}{d}\right)^2 B_\lambda(T_*)\,\Delta\lambda \quad (2)$$

$\eta_*(\lambda,B)$ is the residual star transmission of the interferometer. Its minimum value depends on the star diameter $\Delta\theta_*$ which is partly resolved by the interferometer. It is also impacted by the instrument defaults like the intensity mismatch ($I_2/I_1=1+\varepsilon$) and the residual OPD ($x=2\pi\delta/\lambda$). In a first approximation:

$$\eta_*(\lambda,B) = \left(1+\frac{\varepsilon}{2}\right) - \sqrt{1+\varepsilon}\cos(x)\left(1-\frac{X^2}{8}+\frac{X^4}{192}\right) \quad (3)$$

Assuming statistics on ε and δ ($\langle\varepsilon\rangle$, σ_ε, $\langle\delta\rangle$, σ_δ), one can derive the statistics on I_* ($\langle I_*\rangle$, σ_*) using Monte-Carlo simulations. In the reference case, $\langle I_*\rangle=380$ e^-/s and $\sigma_*=1.8$ e^-/s.

Optics are considered as grey bodies with emissivity $\varepsilon(\lambda)$ and temperature $\langle T_o\rangle$ with stability σ_{TO}. The corresponding flux on the detector can be estimated by:

$$I_{th} = \pi A\left(\frac{a\lambda}{D}\right)^2 \int_{\lambda-\Delta\lambda/2}^{\lambda+\Delta\lambda/2} \eta_q(\lambda)\varepsilon(\lambda)\; B_\lambda(T_o)\, d\lambda \quad (4)$$

The beam etendue is limited to a fraction of the Airy radius: a $1.22\lambda/D$ (a<1). In the reference case I_{th} is completely negligible. At 5 µm, $\langle I_{th}\rangle=0.9$ e^-/s and $\sigma_{th}=0.3$ e^-/s whereas $\langle I_p\rangle=10$ e^-/s.

The detector noise consists in a read out noise (σ_{RON}) and a dark current variation (σ_{dark}) coming from the thermal stability of the detection plane ($\langle T_d\rangle$ and σ_{Td}). A numerical fit of data for Hg-Cd-Te detector assuming a 5 µm upper limit and a 18 µm pixel leads to the following law : $I_{dark}=1.6310^{-35}\, T_d^{19.6}$ e^-/s/pixel.

For a total integration time τ_i, the shot noise is $\sigma_{sh} = \sqrt{\tau_i \sum I_k}$ and the SNR in nulling mode writes:

$$R = \frac{I_p \tau_i}{\sqrt{2}\sqrt{\sigma_{sh}^2 + f\tau_i\sigma_{RON}^2 + (\sigma_*^2 + \sigma_{th}^2 + \sigma_{dark}^2)\tau_i^2}} \quad (5)$$

Some results are illustrated by Fig. 4 which shows the various components of the SNR as function of λ with the nominal set of parameters.

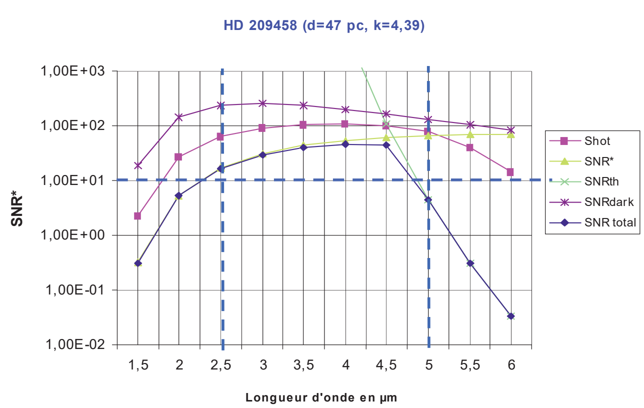

Fig. 4: example of SNR calculation in nulling mode. Parameters : τ_i=10 h, T_p=1400 K, R_p=1.5 , S_p=1, a=1, D=40 cm, R=60, η_o=0.07, η_q=0.6, $\langle T_d\rangle$=55 K, σ_{Td}=0.1 K rms, $\langle T_o\rangle$=100 K, σ_{To}=1 K rms, $\langle 2\pi\delta/\lambda\rangle < 510^{-3}$ rad, $\langle\varepsilon\rangle < 0.01$, σ_δ=2.5 nm rms, σ_ε=0.003 rms, σ_{RON} =10 e^- rms

In the lower part of the wavelength range, the SNR is limited by the nulling stability. It is directly linked to the stability and mean value of the OPD and of the intensity mismatch. Achieving the desired SNR below 2.5 µm would mean a sub nm OPD control what would lead to a much more complex mission. As a compromise between the scientific interest and the mission cost, the lower wavelength limit was set to 2.5 µm which still allows the detection of CH_4, H_2O and CO. In the upper part of the spectrum, the performance is limited by the temperature of the optics and its stability. Again, a system trade-off was performed and reduced the upper limit from 6 µm (initial proposal) to 5 µm to avoid a too complex thermal design. In the middle part, we set the integration time and the detector temperature so that the photon noise and the detector noise only limit the performance for targets farther than 100 pc. The resulting optimized set of parameters is listed in the first column of table 1. Seven objects of the initial list have SNR >10 in the whole spectral range. Five other hot Jupiters have a medium difficulty level with 5 < SNR < 10. Four objects have SNR < 5 and are considered too difficult for the Pegase mission.

Parameter	HJ nulling (1)	BD nulling	Gap V^2 (2)	HJ V^2 (3)
τ_i (h)	10	10	3	30
B/2 (m)	50-200	5-80	50-250	100-400
σ_δ (nm rms)	**2.5**	**2.5**	15	2.5
<x> (rad)	0.001	0.001	0.02	0.005
σ_ε (rms) (point.mas)(4)	0.003 **(30)**	0.003 **(30)**	0.03 (300)	0.005 (50)
<ε>	0.01	0.01	0.1	0.01
σ_{To} (K rms)	1	1	1	1
<To> (K)	100	100	105	100
σ_{Td} (K rms)	**0.1**	**0.1**	**0.1**	**0.1**
$<T_d>$ (K)	**55**	**55**	60	60
RON (e^-)	10	10	50	50
Nbr of targets (5)	12	3	> 100	12

Table 1 : driving parameters in various modes

(1) SNR > 10 in 2.5-5 µm for easy targets, (2) K_{lim}=10, SNR V^2=200, (3) SNR V^2=2000 at 5 µm; 10000 at 2.5 µm (4) intensity mismatch constrains the pointing through fiber coupling [2], (5) in 2005

Similar calculations were performed for the brown dwarfs and for the V^2 mode applied to gap detection in the disks. The V^2 mode can also be applied to hot Jupiters spectral characterization by analysing very small oscillations (0.001 order of magnitude) in the visibility curve and is then an alternative to nulling. The associated constraints on the system parameters are listed in table 1. The hot Jupiters are the most demanding case for the mission, with a very stringent requirement on the stability of the OPD at 2.5 nm rms level. The intensity mismatch translates into a 30 mas pointing stability which is also quite demanding. A 0.1 K temperature stability of the focal plane is required to avoid too important dark current variations. The temperature of the optical bench shall not exceed 100 K with 1 K stability. The V^2 and nulling modes lead to comparable constraints although the V^2 mode slightly relaxes the temperature of the detector and the pointing, but at the price of a longer integration time and longer baselines. The V^2 mode for the detection of gaps in disks is clearly a less demanding objective.

4. – FORMATION FLYING CONTROL

In our study we focused on the last control phase assuming the formation has been previously put in a coarse situation after a manoeuvre or a recovery from a safe mode using radiofrequency (RF) metrology.

4.1 – General principle

Trying to match the pointing and OPD stability requirements from table 1 with a one level control architecture based on continuous actuation at satellite level only means using micro-thrusters and sensors with ultra-high accuracy. The associated technologies are very complex. To reduce costs and risks, we oriented our effort toward more conventional technologies such as impulsive cold gas thrusters and tried to relax the requirements on the spacecrafts attitude and position control. This led us to consider a two level control architecture combining control loops operating at satellite level and fine control loops implemented inside the optical payload. These fine loops have to compensate the external residual movements by corresponding displacements of optical delay lines (ODL) and fast steering mirrors (FSM). They must have a high enough bandpass to reject noises with sufficient efficiency. The limitations of such systems come mainly from undesired high frequency noise such as microvibrations from small mobile parts amplified by structural resonances as already studied in the SIM case for example [11]. A good compromise between the two control stages is a central issue for the feasibility of such a mission.

4.2 – Discontinuous control

As the internal mechanisms have a finite stroke, they can not compensate the spacecrafts movements during the integration time specified in table 1. It has to be split into elementary integration periods during which the vehicles are left drifting under the natural perturbations. Small impulsive manoeuvres are applied between two quiet periods to avoid the saturation of the fine mechanisms. Some relaxation in terms of metrology accuracy becomes possible since the absence of thrusters noise allows the improvement of estimation performances. The corrective manoeuvres will create an OPD shift exceeding the 2.5 nm level and interrupting the scientific observation for a short time (loss of the fine fringe tracking but the OPD remains in the coherence length). The key point is therefore the duration of the quiet periods and the scientists have agreed so far to split the observations in 100 s slices.

4.3 – Fine control loops

As the external disturbances introduced by the absolute positioning of the baseline with respect to the observed astronomical object can only be measured from the light emitted by the object itself, the fine correction stage has to be based on the light emitted by the star around which orbits the weak companion of interest. Maximizing the flux on the fine sensors is of critical importance for the ultimate nulling performance.

The OPD loop is based on a fringe sensor (FS) and an optical delay line (ODL). The fine pointing loop is based on a precise field relative angle sensor (FRAS) and fast steering mirrors (FSM). The fine sensors are included in the optical payload and use part of the flux collected by the beam compressors. See a more precise description in [2].

The estimated performances were computed for piston and tip/tilt [2]. The analysis shows that the best spectral domain is the visible. This is an important result since efficient space-qualified detectors are available in the visible and this saves all the IR photons for the scientific instrument.

As far as the OPD is concerned, an integration time of about 20 ms is sufficient for most targets, i. e. a correction frequency from around 50 Hz (up to 200 Hz for a few targets). This should be sufficient to control OPD contributors at low frequency (residual speed, differential solar pressure,…) or at high frequency (microvibrations) since their amplitude is smaller and advanced control techniques (such as Kalman filtering) can be used for known disturbances (constant acceleration, sinusoidal harmonics). Acquisition of the fringes is possible in the visible spectral range using realistic parameters for the real-time processor and an external OPD drift up to 150-200 µm/s.

Assuming that the coupling efficiency follows the Strehl approximation [9] and a mean intensity mismatch of 10^{-2}, a specification of around 30 mas per axis for the pointing accuracy has been evaluated to fulfil the specification on ε from table 1. It appears that the exposure time can be smaller than a few ms for most of the stars.

4.4 – Satellite control

Environment perturbations: In L2 environment, the dominant disturbances come from the solar radiation pressure that produces differential forces and torques due to non identical surface to mass ratios and lever arms between the center of pressure and the center of mass. It has be shown that the attitude bounds will be exceeded much faster than position bounds in absence of control: a 5 mm drift occurs after 1000 s whereas a 10'' pointing error is reached after 100 s in the worst case with $\beta = 30°$.

Hybrid architecture: The impulsive control approach leads to the problem of synchronising the gas pulses. The high number of degrees of freedom combined with their associated dynamics would require a complex synchronization algorithm so as to ensure the 100 s quiet period. To avoid it we chose an hybrid architecture based on reaction wheels to ensure pointing requirements of the siderostats. The pointing of the combiner and the relative positioning are still performed with cold gas systems. A preliminary analysis shows that the microvibrations generated by the reaction wheels on the siderostats are consistent with the requirements on pointing and OPD stability. The stiff structure of the siderostats and the light reaction wheel are favourable factors. Actual studies are focusing on this matter and on the torque fluctuations which need to be further investigated.

Platforms control objectives: The first goal is to keep the internal mechanisms within their working domains during the elementary integration of 100 s. This requires that the external OPD stays below the assumed delay line stroke. In parallel the cumulated pointing errors of the combiner and the siderostat must ensure that the beam deviations remain within the FSM stroke. As the use of the FRAS and reaction wheels will allow a relative pointing control of the siderostats at 1" accuracy level, we found that the inertial pointing of the combiner can be relaxed to +/- 5 to 10", depending on the exact value of the angular magnification M and the FSM effective stroke.

Another key function of the control is to lead the formation from a deployment state to a fine stabilized state. which requires that the external OPD velocity is less than 100-150 µm/s (with some margins w.r.t. section 4.3 result). Such a requirement applies to the cumulated effects of various degrees of freedom (DOF) both in translation and rotation. An allocation is needed between the various terms. As a preliminary rule, we specified a equivalent velocity control accuracy of 10 to 20 µm/s rms on each DOF of interest.

Calibration process: As the initial cumulated bias of the various DOF metrologies used to estimate the external OPD will exceed the stroke of the ODL, a calibration process is needed. It is foreseen to scan the OPD using the movement of one siderostat in order to estimate this cumulated bias with a precision roughly equal to the coherence length of the science interferograms (about 100 µm). Consequently, there is no need for a very accurate distance sensor.

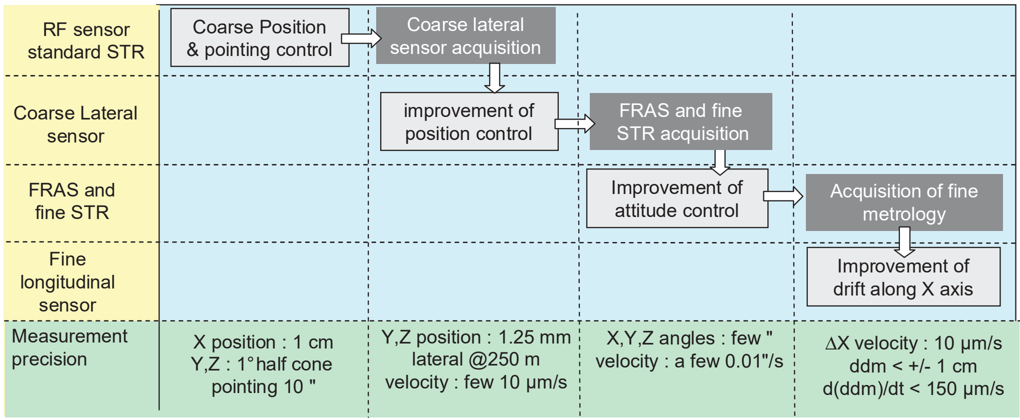

Fig. 5: sequencing of the metrologies

Filtering: Filtering algorithms using the predictable movement laws in L2 environment will be used to relax the resolution of the sensors imposed by the formation damping requirement. A preliminary work performed at ONERA under CNES R & D contract estimates that a factor 10 to 100 can be saved this way.

Sensors specifications: the metrology was defined to fulfil the positioning and stability requirements with the use of filtering and initial calibration of the OPD uncertainty. For the translation DOF, biases of 1 cm are acceptable on the absolute position measured by the sensors (RF metrology along the X axis, 10" bias on lateral sensor). The relative displacements must be measured with 0.1 mm to 1 mm resolution at 10 Hz, depending on the exact filtering performance. Along the X axis, this may be achieved by the RF metrology in an optimistic case but to be more conservative, the nominal set up will include a simple laser telemeter (resolution of 1 fringe is sufficient) which could be of the MOUSE Type [12]. Along the other axes, the lateral sensor should have a 0.1 to 1 arcsec resolution. According to a first study performed by the French company Sodern under CNES R & D contract, this is possible using small cameras on the combiner and a laser diode based illuminator on each siderostat (λ=850 nm). As far as pointing is concerned, a fine star tracker of the arcsec class is very probably needed in the payload of the combiner (damping requirements).

Propulsion specification: The analysis shows that classical cold gas thrusters with a minimum impulse bit (MIB) of 0.05 m.N.s are needed.

Sensors and modes sequence: Fig. 5 illustrates the foreseen sequencing of the various metrologies and control stages.

5. – OVERVIEW OF THE SPACE SEGMENT

5.1 – Optical Payload

A possible optical layout is illustrated by Fig. 6. To reduce the cost a major system choice was to use flat 45° mirrors (M1) on the siderostat instead of afocal telescopes. The beam compressors (M2, M3) are then located on the beam combiner and are axial to be more compact.

Many constraints apply on the design. We first had to cope with a limited volume (120 x 120 x 60 cm) because of the system choice to fit into a Soyuz fairing without deployable sun shields (see 5.5). This leads to limit the collecting diameter to D< 40cm. Second, the reliability in space environment imposes the redundancy of all mechanisms. That's why each arm has its own ODL (M5, M6, cat's eye type) which are grouped with the FSM on a supporting plate. Then, we minimized the number of components in order to reduce the complexity and maximize the optical transmission. Another guideline was to minimize the coupling of various degrees of freedom, either at satellite level or in the payload itself. That's why we imposed the stop on FSM (M7) so that the impact of the tip/tilt correction on the OPD is minimized. Last, the two arms of the interferometer shall have a maximum symmetry w.r.t. reflections to minimize the differential polarization effects. The FSM are an exception to this rule as they will have different positions to correct different pointing errors of each siderostat. We estimated that a +/-60" stroke leads to a nulling perturbation less than 10^{-8}.

The other major points of the pre-design are:

- M1/M4 form an achromatic π phase shifter using field reversal by reflections [13], that could be complemented by dispersing prisms if needed [14],
- A modified Mach-Zender provides a full symmetric and achromatic recombination for the nulled outputs [15] and a spatial modulation for the SF [2],
- Both MMZ are superposed to minimize the stability problems between metrology and science [14],
- The outputs of the IR MMZ is injected into monomode fibers made of fluorid glasses that feed a 55 K detection module based on Hg-Cd-Te detectors,

- The visible part of the spectrum is divided between the FS and the FRAS (exact allocation is TBD)
- The +Y part of the bench will be used to implement fine sensors required by the GNC (see Fig.9 and 4.4),
- The structure of the optical bench will use ultra-stable materials such as Sic or Cesic.

A more detailed description of the optical payload may be found in [2]. The main global characteristics of the payload are listed in table 2.

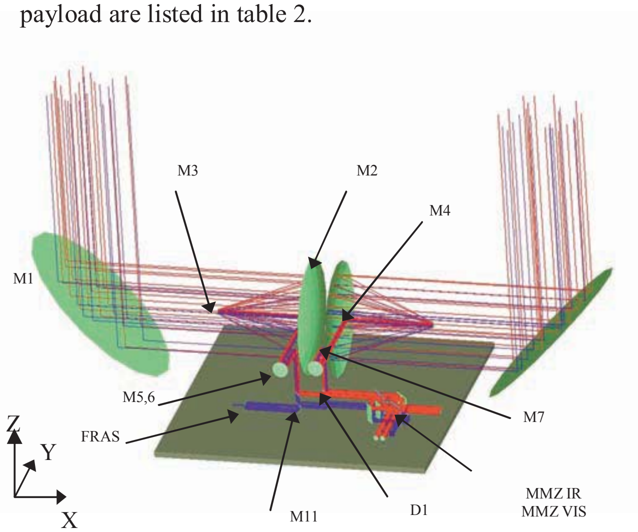

Fig. 6: preliminary optical layout

Parameter	Value
Mass	70 kg
Dimensions	120 x 120 x 60 cm
IR optical transmission(*)	7 % 2.5-5µm
FRAS optical transmission(*)	12 % 0.6- 1.0 µm
SF optical transmission(*)	8% 0.6- 1.0 µm
Collector diameter	40 cm
Mirror coatings	Gold, $\lambda_{vis}/20$
Effective focal length	1.800 m
Optical bench Temperature	100 +/- 1 K
Detector temperature	55 +/- 0.1 K
Single mode fibers	fluorid glasses
Science detectors	Hg-Cd-Te
FRAS resolution	10 mas
Magnification of afocal	15 to 20

Table 2 : Main characteristics of the payload (*)includes beamsplitters, 0.7 fiber coupling, assumes 0.95 reflectivity, does not include quantum efficiency

5.2 – Orbit selection

A trade-off was performed between High Elliptical Orbits (HEO) and Sun-Earth system L2 point orbits (L2). Given all the constraints an eight days period orbit with a 40 000 km high perigee and a 285 000 km high apogee was selected in the HEO case. Although the gravity gradient is compatible with the mission on more than 90% of the orbit, it was not possible to prove at the stage of pre-design whether the variations of the heat flux due to Earth were compatible or not with the payload thermal stability needs (see 5.4). As the cost difference with the L2 option is not so significant, the HEO orbit was not chosen as the baseline for our study but the trade-off is not completely closed.

Two kinds of orbits have been investigated at L2: the halo and Lissajous orbits. A Lissajous orbit was eventually retained in the study because it is much easier to operate and the total ΔV needed is not more important than the one for a halo orbit. The chosen orbit minimizes the requested injection ΔV. Its parameters in the synodic plane are 250 000 km (x) / 673 000 km (y). In this plane it has an instable motion with a period of ~177,6 days. Out of this plane the motion is stable with a period of 184 days.

5.3 – Operations and mission duration

The critical operations are the rotation of the formation, the adjustment of the size of the baseline and the change of target. At L2 point, a typical telemetry and telecommand (TTC) session will last 8 hours. System wise it has been chosen to perform the critical operations under the monitoring of the ground segment. As a consequence during the TTC session the satellites will move to the next position with velocities of a few cm/s, download the telemetry and receive the flight program for the next day. A typical 6 days long sequence is illustrated on Fig. 7 in the nulling mode for hot Jupiters or brown dwarfs. Assuming 20 objects of each type, 240 days are needed to cover the scientific mission. Adding another 120 days for the observation of the disks, one gets a total scientific mission duration of one year. Considering a mean availability of the system of 0.75, the total mission duration is estimated to 2.5 years, including a 4 months transfer phase, a 4 months commissioning phase and a 6 months margin for additional programs.

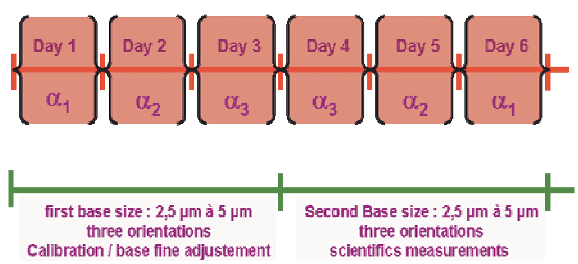

Fig. 7: typical observation sequence (Hot Jupiters)

5.4 – Thermal control

The system choice is to use a passive system to avoid the mechanical perturbations of the OPD by active cryogenic devices. Due to the earth albedo, maintaining the 0.1 K stability on the detector plane during a sufficient part of the HEO with a passive design seems difficult. The equivalent mean well temperature is 45 K as compared to 3 K at L2. The

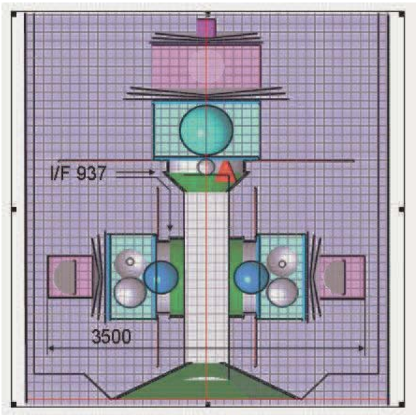

Fig. 8: launch configuration

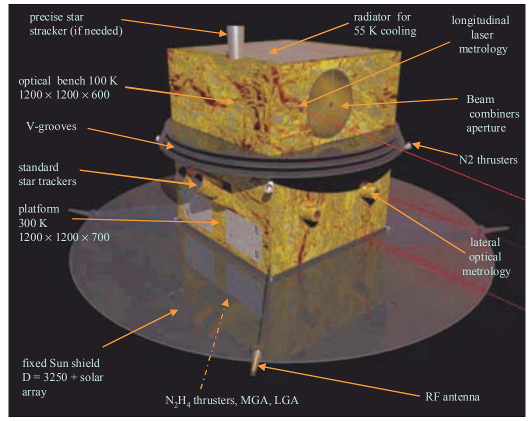

Fig. 9: layout of the combiner satellite

required radiator would be white painted with a 4.5 m^2 surface to evacuate 1 W. The required stability would impose a quite complex sun shield around the payload due to the various pointing configurations along the seasons and the orbit. Last, the formation would have to avoid the high perturbation peak near the perigee with a special de-pointing configuration. A detailed thermal analysis is needed to further investigate the feasibility of this option.

In the L2 case, the thermal control is based on a high decoupling between the service module (300 K) and the optical payload (100 K) using V-grooves systems. The decoupling of the detector stage (55 K) w.r.t. the optical bench is TBD. The radiator is dark painted and the surface to evacuate 1 W is only 2 m^2. The V-grooves and the payload have to be protected from the direct sun light by sun shields assuming anti-solar pointing with a maximum depointing angle of 30°.

5.5 –Mechanical configuration

After a detailed analysis, the use of existent platforms suggested in the initial CNES call for proposals proved to be inadequate for Pegase. The mechanical architecture is then based on dedicated platforms. To reduce the costs, the choice was made to use one single Soyuz launcher and to avoid deployable sun shields. The internal diameter of the launcher fairing becomes a major constraint. A compromise had to be made between the diameter of the collectors, the size of the vehicles, the allowable depointing angle β. We found that $\beta<30°$ gives access to more than 90% of the identified objects and is compatible with the Soyuz fairing with fixed sun shields if D<40 cm and a special structure is used to accommodate the three satellites under the Soyuz fairing. A solution based on the Sylda proved to be less efficient. The retained configuration is illustrated by Fig. 8. Fig. 9 outlines the combiner.

5.6 – Propulsion

The nominal solution retained for the formation flying propulsion is an impulsive cold gas (N_2) system based on existing technology (10 mN thrusters from Marotta UK) with a MIB reduction down to 50 µN.s. That does not represent a strong technology push (a gain factor of 10 w.r.t. Grace thruster resolution) and seems affordable by reducing the minimal path of the thrusters divergent (today's diameter is 0.26 mm), limiting the pulse duration and reducing the thrusters admission pressure (today it is roughly 1.3 bars for Marotta technology). Assuming 70 % efficiency, the total ΔV needed for the formation control (change of target, rotation and sizing of the formation), the fine orbit control and the failure detection and recovery system is 25 m/s for the combiner and 17 m/s for each siderostat. For high ΔV (injection, rough positioning) the solution retained is a classical hydrazine system. The launcher corrections, the injection on the orbit and the orbital manoeuvres require about 92 m/s ΔV on each spacecraft (98% efficiency).

5.7 – Telecommunication

From a communication point of view, the formation is considered nominally as one spacecraft with a 600 Mbits/day total telemetry. The main link uses the X-band and 15 m ground antennas to communicate with the combiner equipped with 2 low gain antennas and 2 medium gain antennas. The data from the siderostats are collected through the intersatellite link which uses the RF metrology. Back-up links are available on the siderostats for the safe mode operations where independent access to each satellite is possible.

5.8 – Mass and Power budgets

The solar arrays are fixed and located at the back of the sun shields. Assuming 60 % of AsGa3J solar cells, 40 % of optical solar reflectors and a 0.7 fill factor, the available powers are 260 W for the siderostat and 770 W for the beam combiner which is largely sufficient to cover the payload and platforms needs. The mass budget was build upon a detailed analysis at component and sub-system levels using CNES internal databases. It also includes all liquid propellants. A 5 to 20 % margin is applied at equipment level depending on the maturity and a global 30% system margin applies. The resulting mass estimates are 350 kg for each siderostat and 700 kg for the combiner. The total launch mass is estimated to 1785 kg which leaves a 13% margin w.r.t. the Soyuz performance (2050 kg).

5.9 – Cost estimation

At this stage, the cost estimation process of such a challenging mission is very difficult and subject to a lot of uncertainties. The difficulty is furthermore amplified by the free flying technology which is a major innovation without any prior mission as a reference. Rough order of magnitude (ROM) costs have been estimated thanks to an analytical method with appropriate margins depending on the technology maturity level. In addition, parallel costs databases for similar payloads and platforms have been used. As an example, the IASI interferometric payload has an equivalent final cost of 1 ME/kg which is very near from the figure obtained with the analytical method on the combiner payload. Assuming some other simpler mission validates the first level of formation flying, the total development plan (ABCD phases) is estimated to expand over a 8 to 9 years time period. Assuming a development mainly performed in the industry, the estimated ROM external cost is 320 ME +/- 20 % (payload 70, launch 50, operations 20, combiner 110, siderostats 70 ME). An additional 10% margin is taken to calculate the maximum cost. These figures are comparable with the estimations of NASA for similar missions (FKSI [16], early version of Starlight).

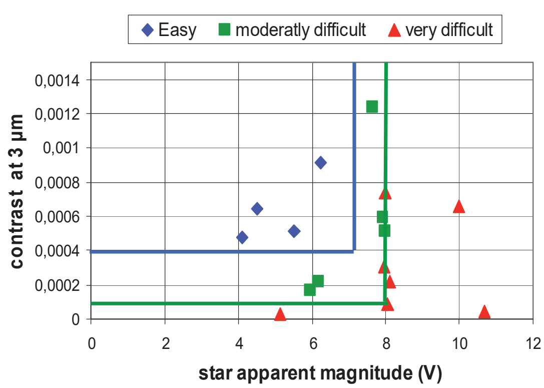

Fig. 10: performance domain. Diamonds: easy HJ, squares: intermediate difficulty HJ, triangles: impossible with current assumptions. The OPD stability imposes contrast > 10^4 The FS requires central stars brighter than V=8.

7. – CONCLUSION

Fig. 10 summarizes the estimated main performances of the Pegase mission for the spectroscopy in the nulling mode. Today, more than 12 objects (HJ and BD) can be found in this domain and more will come in the next years. With many possible other programs, such as the detection of gaps in protoplanetary disks, the expected scientific return is very valuable.

From an engineering point of view, this phase 0 study only gives the outlines of what could be the Pegase mission. Some major trade-offs are still open and many subjects remain of course to be investigated in much more details during a future phase A. Nevertheless, the resulting first picture is attractive and it seems to us that this mission could be a good compromise between the scientific interest and the technological challenge when placed into an international roadmap toward free flying interferometry in space. We therefore think that Pegase can be proposed to ESA/NASA as an intermediate pathfinder mission before TPF-I/Darwin if the planned funding for the next decade allows such an option. The future R and D work will focus on a breadboard of the payload including the nulling interferometer and the fine control loops [2].

8. - REFERENCES

1. Leyre X. et al., « First formation flying interferometric mission including a Bracewell nulling », 2nd International Symposium on Formation Flying, Washington, sept. 2004
2. Cassaing et al., « Towards a laboratory breadboard for PEGASE, the DARWIN pathfinder », proceedings of ICSO 2006 conference.
3. Sudarsky et al, « Theoretical Spectra and Atmospheres of Extrasolar Giant Planets », ApJ, Vol. 588, p 1121-1148, 2003
4. Barman T.S. et al, « Phase-Dependent Properties of Extrasolar Planet Atmospheres », ApJ, Volume 632, Issue 2, pp. 1132-1139, 2005
5. Bracewell R.N., « Detecting non solar planets by spinning infrared interferometer », Nature, 274, p.780, 1978
6. Léger A. et al., « Could we search for primitive life on extrasolar planets in the near future ? The Darwin project », Icarus 123, 249-255, 1996
7. Angel J.R.P., Woolf N.J., « An imaging nulling interfero. to study extrasolar planets », AJ, 475 :373, 1997
8. Ollivier M. and Mariotti J.M. « Improvement in the rejection rate of a nulling interferometer by spatial filtering », Applied Optics, Vol 36, N° 22, p 5340-5346, 1997
9. Ruilier C. and Cassaing F. « Coupling of large telescope and single-mode waveguides » JOSA, Vol 18, N° 1, p 143-149, 2001
10. Ch. Leinert et al., « The 1997 reference for diffuse night sky brightness», A&A SS, 127 1-99, 1998
11. Miller D.W. et al., « Integrated dynamics and controls modelling for the Space Interferometry Mission (SIM) », in IEEE Aerospace Conference, vol. 4, p2089-2102 2001
12. Le Duigou J.M., Poupinet A., « The MOUSE II sensors for longitudinal measurements », proceedings OPTRO 2005,
13. Serabyn E. et al., Applied Optics, Vol. 38, No 34, pp 7128-7132, 1999
14. Brachet F., « Etude et développement d'un déphaseur achromatique pour l'interférométrie en frange noire » thèse de doctorat de l'université Paris-Sud (XI), 2005
15. Serabyn E. and Colavita M.M., « Fully symmetric nulling beam combiners », Applied Optics, Vol.40, No 10, pp 1668-1671, 2001
16. W.C. Danchi et al, « The Fourier-Kelvin stellar interferometer : a practical interferometer for the detection and characterization of extra-solar giant planets », SPIE Vol 5491 p236 à 241, 2004